Drug Design, Development and Therapy

Dovepress
Taylor & Francis Group

Open Access Full Text Article

ORIGINAL RESEARCH

Xian Huang Fang Inhibits the PKCδ/MAPK Signaling Pathway to Attenuate Renal Tubular Epithelial Cell Senescence and Thereby Delay Renal Interstitial Fibrosis

Yanru Wang[1–4], Minghai Shao[1–4], Tingting Li[1–4], Xiu Du[1–4], Kanjun Chen[5], Lin Xu[1–4]

[1]Department of Nephrology, Shuguang Hospital Affiliated to Shanghai University of Traditional Chinese Medicine, Shanghai, 201203, People's Republic of China; [2]Key Laboratory of Liver and Kidney Diseases, Ministry of Education, Shanghai University of Traditional Chinese Medicine, Shanghai, 201203, People's Republic of China; [3]TCM Institute of Kidney Disease, Shanghai University of Traditional Chinese Medicine, Shanghai, 201203, People's Republic of China; [4]Shanghai Key Laboratory of Traditional Chinese Clinical Medicine, Shanghai University of Traditional Chinese Medicine, Shanghai, 201203, People's Republic of China; [5]Department of Traditional Chinese Medicine, Shuguang Hospital Affiliated to Shanghai University of Traditional Chinese Medicine, Shanghai, 201203, People's Republic of China

Correspondence: Lin Xu, Department of Nephrology, Shuguang Hospital Affiliated to Shanghai University of Traditional Chinese Medicine, No. 528 Zhangheng Road, Pudong District, Shanghai, 201203, People's Republic of China, Email xulin-02@163.com

Background: The Chinese herbal medicine compound Xian Huang Fang (XHF) protects renal function and delays the progression of chronic kidney disease (CKD). Currently, XHF has been found to alleviate renal interstitial fibrosis, but the specific mechanism is still unclear, and its underlying molecular mechanism needs to be further elucidated.

Purpose: The objective of this study was to investigate the protective effects of XHF against renal fibrosis and the underlying mechanisms.

Methods: Chemical profiling of the reconstituted XHF freeze-dried powder was performed using ultra-high-performance liquid chromatography coupled with quadrupole-Orbitrap high-resolution mass spectrometry (UHPLC-Q-Orbitrap HRMS). Chronic renal failure model was established via 5/6 nephrectomy (A/I), and renal tubular epithelial (HK-2) cell fibrosis was induced by 5 ng/mL Transforming growth factor β1 (TGF-β1). Mechanisms were evaluated using network pharmacology, histopathology, Western blotting, immunofluorescence (IF), and senescence-associated β-galactosidase (SA-β-gal) staining.

Results: XHF significantly ameliorated renal injury, reduced inflammatory infiltration in the renal interstitium, and effectively improved renal interstitial fibrosis (RIF) in 5/6 nephrectomy (A/I) model rats. Network analysis revealed Protein Kinase C delta (PKCδ) as a key target; XHF inhibited the phosphorylation of PKCδ (Tyr311), subsequently downregulating phosphorylated (p)-p38, p-ERK, p-JNK, and p-NF-κB both in vivo and in vitro. Furthermore, it upregulated the expression of the cell proliferation marker Ki67, while suppressing senescence markers (SA-β-gal activity, p21) and the senescence-associated secretory phenotype (SASP) factors (eg, IL-6).

Conclusion: XHF alleviates renal interstitial fibrosis by inhibiting the PKCδ/MAPK signaling pathway, thereby reducing the senescence of renal tubular epithelial cells.

Keywords: XHF, CKD, PKCδ, cellular senescence, SASP, network pharmacology

Introduction

CKD is an important factor contributing to the global increase in the incidence of noninfectious diseases and the increase in human mortality.[1,2] RIF is a common pathway and a major pathological manifestation of the progression of CKD from different causes.[3] Injured renal tubular epithelial cells (RTECs), the primary cellular component of the tubulointerstitium, exhibit impaired repair capacity. This manifests as cell cycle arrest, partial epithelial-mesenchymal transition (EMT), and critically, the acquisition of a pathological cellular senescence phenotype.[4–6] Factors such as hypoxia, metabolic stress,

Received: 12 February 2025
Accepted: 5 August 2025
Published: 13 August 2025

and persistent injury can trigger this damaging senescent state in RTECs.[7,8] Given the lack of effective therapies to halt tubular damage and mitigate established fibrosis, novel strategies targeting key drivers like pathological cellular senescence are urgently needed.

Notably, cellular senescence is increasingly recognized not only as a consequence of aging but also as a potent driver of fibrosis in progressive CKD.[9] Cellular senescence has been observed in renal fibrosis models, including the 5/6 nephrectomy mouse model.[10,11] The SASP creates a deleterious microenvironment that perpetuates inflammation, promotes fibroblast activation, and accelerates ECM deposition, thereby driving RIF progression,[12,13] and its activity can be modulated by upstream kinases, including members of the MAPK family (p38, ERK, JNK).[14,15] Targeting pathways that regulate this pathological senescence response, therefore, holds promise for interrupting the vicious cycle of inflammation and fibrosis in CKD.

The herbal combination of Rheum palmatum (Da huang) and Epimedium (Yin yang huo), referred to here as Xian Huang Fang (XHF), is a clinically used pairing in traditional Chinese medicine (TCM) for managing CKD.[16] Bioactive components derived from its constituent herbs, such as icariin (Epimedium) and emodin (Rheum palmatum), possess documented anti–inflammatory, antioxidant, and anti-fibrotic properties.[17,18] For example, our laboratory has found that icariin has been proven to mitigate renal fibrosis by inhibiting the activation of fibroblasts, while emodin can improve tubulointerstitial fibrosis in obstructed kidneys by inhibiting EZH2.[19,20] While these studies highlight the potential of XHF and its components against fibrosis, the precise molecular mechanisms, particularly concerning its potential impact on the critical pathological process of cellular senescence within the fibrotic kidney, remain largely unexplored.

Therefore, this study investigated whether XHF alleviates RIF by targeting pathological cellular senescence. To elucidate the underlying mechanisms of XHF treatment, we integrated network pharmacology to predict PKCδ as a candidate core target and validated its role in both in vivo and in vitro renal fibrosis models exhibiting senescent characteristics. Furthermore, we explored the molecular mechanisms behind its effects, with special emphasis on the relationship between XHF and fibrosis-associated cellular senescence. The results of this study can inform further research on the improvement of RIF by XHF.

Materials and Methods

Preparation of XHF and Quality Control Analysis

XHF consists of 15 g *Rheum palmatum* and 15 g *Epimedium* (Lot No.160718HY/161228HX). The raw herbs for the preparation of XHF were provided by the Department of Pharmacy, Shuguang Hospital, Shanghai University of Traditional Chinese Medicine, Shanghai, China. The samples were thoroughly verified by Professor Yang Tao, a botanist from the Affiliated Shuguang Hospital of Shanghai University of Traditional Chinese Medicine, in accordance with the Chinese Pharmacopoeia. XHF was prepared by cutting the herbs into small pieces, mixing them, and boiling the mixture at 100 °C for 1.5 h. The resulting supernatant was concentrated under vacuum in a rotary evaporator, and after ultrafiltration, the concentrated extract was lyophilized to obtain a freeze-dried powder for storage, which was used for both in vivo and in vitro interventions. Losartan potassium tablets (Hangzhou Merck Sharp & Dohme Pharmaceutical Co., Ltd., batch no. N008670, specification: 50 mg/tablet) were formulated as a 5.0 mg/mL suspension. Chemical profiling was performed using ultra-high-performance liquid chromatography coupled to quadrupole-Orbitrap high-resolution mass spectrometry (UHPLC-Q-Orbitrap HRMS; Dionex UltiMate 3000 UHPLC system coupled to a Thermo Q Exactive MS, Syncronis C18 column, 1.7 μm, 2.1×100 mm). Chromatographic separation was achieved with a gradient of 0.1% (v/v) formic acid in water (mobile phase A) and acetonitrile (mobile phase B) as follows: 0–12 min, 95% A; 12–14 min, linear gradient to 5% A; 14.1–16 min, 95% A. The flow rate was 0.3 mL/min with an injection volume of 3 μL. MS detection parameters: Full MS/dd-MS² mode; scan range: m/z 150–1200; resolution: 70,000 (Full MS), 17,500 (MS²); H-ESI source: spray voltage +3.2 kV (positive), −2.8 kV (negative); capillary temperature: 320 °C; NCE: stepped 35% and 50%.

Reagents and Antibodies

TGF-β1 (0922209–1, Peprotech), FN (ab45688, Abcam), anti-GAPDH (60,004-1-1g, Proteintech), anti-vimentin (SC6260, Santa Cruz), anti-α-smooth muscle actin (α-SMA) (ab124964, Abcam), anti-Ki67 (ab16667, Abcam), anti-p-NF-κB p65 (3033, CST), anti-phospho-PKCδ (Tyr311) (#2055, CST), anti-PKCδ (9616T, CST), anti-p-JNK (sc-6254, Santa Cruz), anti-JNK (sc-7345, Santa Cruz), anti-p-ERK (sc-7383, Santa Cruz), anti-ERK (4695T, CST), anti-p-p38 (4511T, CST), anti-p38 (8690T, CST), anti-OAT3 (bs-0609R, Bioss), anti-AQP1 (ab168387, Abcam), anti-CHOP (sc-7351, Santa Cruz), anti-ATP1B1 (15,192-1-AP, Proteintech), and HSPA5/BiP/GRP78 (sc-13539, Santa Cruz) were used.

Animals

The animal study was reviewed and approved by the Animal Ethics Committee of Shanghai University of Traditional Chinese Medicine (PZSHUTCMSZY201707003). Sprague–Dawley (SD) rats (male, 8 weeks old, weighing 180–220 g) were purchased from Shanghai SLAC Laboratory Animal Co., Ltd. [number: SCXK (Hu) 2022-0004]. All the rats were housed under SPF conditions with a constant room temperature of 20–25 °C, a relative humidity of 50%-55%, and a 12 h light/12 h dark cycle under SPF conditions. After one week of adaptation, 5/6 (A/I) nephrectomies were performed as follows.[21] Four weeks after surgery, 40 rats with successful modeling were randomly divided into four groups: the 5/6 (A/I) group (equal distilled water), the (Losartan)LOS group (50 mg/kg), the medium-dose XHF (XHFM) and high-dose XHF (XHFH) groups (2.7 and 5.4 g/kg). After 8 weeks of drug administration, all the rats were injected intraperitoneally with pentobarbital sodium (40 mg/kg). In addition, regarding the care of laboratory animals, we strictly adhere to the Guidelines on Laboratory Animal Welfare and Ethics issued by the Ministry of Science and Technology of the People's Republic of China.

HE, Masson and Sirius-Red Staining

After harvesting, the kidney tissues of the rats were fixed in 4% paraformaldehyde buffer and embedded in paraffin. The 3μm kidney tissue sections were stained with HE, Masson's trichrome and Sirius red according to the staining instructions. The pathological results were observed at ×200 magnification.

Network Pharmacology

The TCMSP database (https://tcmsp.91medicine.cn) was used to search for the active ingredients of each component of the full formula, and then, the chemical composition was entered into the PubChem database (https://pubchem.ncbi.nlm.nih.gov/) to obtain the SMILES numbers of the drug components, which were entered into the SwissTargetPrediction website (http://www.swisstargetprediction.ch/) for target prediction. The keyword "CKD" was used in the GeneCards (https://www.genecards.org/), OMIM (http://www.omim.org/) and DisGeNET (http://www.disgenet.org) databases for disease prediction, and the data were merged and deduplicated. The VennyGeneCards (https://www.genecards.org/) website was subsequently used to take the intersection of XHF drugs and CKD targets to obtain the drug–disease intersection targets. The overlapping targets were imported into GeneCards (https://www.genecards.org/). Similarly, overlapping targets between XHF and CKD-related targets were obtained and uploaded to STRING (http://string-db.org/) for protein–protein interaction analysis, and a protein–protein interaction (PPI) network was constructed by Cytoscape 3.8.2. Finally, the core target information was entered into the DAVID database for GO function and KEGG pathway analysis.

Cell Culture

Human renal tubular epithelial (HK-2) cells were purchased from the Cell Culture Bank of the Chinese Academy of Sciences. Routine cell culture was performed with DMEM/F-12 (PM150310, Pricella) medium containing 10% fetal bovine serum (PYG0109, Boster) and 1% penicillin/streptomycin solution (SV30010, Cytiva), and the mixture was incubated at 37 °C in a 5% CO_2 incubator. The cells were cultured in a 6-well plate. HK-2 cells were inoculated into 6-well plates, and when the cell density reached 60%-80%, the cells were starved with 0.5% fetal bovine serum and 1% penicillin/streptomycin in DMEM/F-12 medium. After 12 h, 1 μM rottlerin was added,[22] and 5 ng/mL TGF-β1 (PeproTech, 100–21, Rocky Hill, NJ, USA) was added after 1 h. Various

concentrations of XHF were added immediately after the addition of TGF-β1. The cells were cultured for 24 h after treatment, and the cell supernatants were collected for subsequent experimental manipulations.

CCK-8 Viability Assays

A CCK-8 assay (40203ES76, Yeasen, Shanghai, China) was used to evaluate the cell viability of HK-2 cells in vitro. First, 8×10^3 cells were seeded into each well of a 96-well plate and incubated with different concentrations of TGF-β1 for 48 h. In a separate set of experiments, cells were incubated with different concentrations of XHF for 48 h. Subsequently, 10% CCK-8 reagent was added to each well and incubated at 37 °C for 1 h. Absorbance at 450 nm was measured using a multimode microplate reader (CYTATION3, BioTek, USA).

Western Blot Analysis

Kidney tissues and cells were lysed with RIPA buffer containing 1% PMSF. Protein concentrations were then quantified via the BCA method, followed by electrophoresis on a 12% SDS–PAGE gel. The membranes were then spun under wet-turn conditions for 2 h, immersed in 5% skim milk powder for 1 h, and probed with primary antibody and HRP-conjugated secondary antibody (1:1000; Beyotime; Shanghai, China). The bands were detected by enhanced chemiluminescence (ECL) (180–501 ECL, Tanon, China). The bands were analyzed quantitatively using ImageJ software.

IF Staining

The After paraformaldehyde fixation, treated HK-2 cells underwent immunostaining with anti-Ki-67 (1:400) and anti-vimentin (1:400) primary antibodies as specified by the supplier. Following incubation with FITC-tagged secondary antibody (2 h, RT), imaging was conducted on a Leica DMi8 fluorescence system.

SA-β-gal Staining

The β-galactosidase staining fixative was configured according to the product specification (SA-β-gal, GP1072, Servicebio) for the SA-β-gal assay, and the prepared tissue cryosections and cultured cells in 6-well plates were added to the configured β-galactosidase staining fixative for 15 min. The staining fixative was then discarded, and the cells were washed 3 times with PBS for 2 min each. The cells were incubated with SA-β-gal staining solution overnight at a constant temperature. After the positive cells were stained, the staining solution was removed, and the cells were washed twice with PBS and twice with purified water, stained with Nucleic Fast Red staining solution for 3 min at room temperature and then washed three times with water. The blue deposits in the cytoplasm of the cells were observed under a light microscope.

Statistical Analysis

All the data are presented as the means ± standard deviations (SD) and were analyzed via one-way analysis of variance with least significant difference (LSD)-*t* test for multiple comparisons using SPSS software (version 25.0, SPSS, Inc., Chicago, USA). $p < 0.05$ was considered statistically significant.

Results

UHPLC-Q-Orbitrap HRMS Analysis of XHF

XHF was formulated with 15 g *Rheum palmatum* and 15 g *Epimedium* (Table 1). The decocted mixture was lyophilized as standardized powder. Chemical profiling using UHPLC-Q-Orbitrap HRMS (Dionex UltiMate 3000; Q Exactive MS;

Table 1 Herbal Composition of XHF

Chinese Name	English Name	Latin Name	Family	Part Used
Da Huang	Rheum palmatum	*Rheum palmatum L.*	Polygonaceae	Root
Yin Yang Huo	Epimedium	*Epimedium brevicornum Maxim.*	Berberidaceae	Leaf

Syncronis C18 column) identified six characteristic constituents in the total ion chromatogram (Figure 1): aloe-emodin, emodin, rhein, chrysophanol, physcion, and icariin.

XHF Attenuates the Progression of 5/6 (A/I)-Induced Renal Fibrosis

To investigate the effect of XHF on renal fibrosis in CKD, we established a rat model of CKD by 5/6 nephrectomy (A/I), after which the rats were treated with different doses of XHF and LOS for 8 weeks. First, Compared with the sham group, the model group showed significantly elevated serum Scr and UACR levels, indicating renal injury. XHF treatment markedly reduced these parameters (Figure 2A and B). Moreover, serum IL-6 and TNF-α levels were increased in the model group versus the sham group, confirming an inflammatory response, whereas XHF markedly decreased these cytokines relative to the model group, underscoring its anti-inflammatory effect (Figure 2C and D). We also analyzed the effects of XHF and LOS administration on renal histopathological changes in the rats with CKD using H&E, Masson's and Sirius red staining. H&E staining revealed that the morphology of the renal tubules and interstitium was essentially normal in the control group of rats. Compared with that in the sham group, renal tubular epithelial cell inflammatory cell infiltration was significantly greater in the model group, with renal tubular vacuolar degeneration and basement membrane thickening, and the model group presented severe renal pathological damage. XHF treatment significantly ameliorated these pathological changes compared to the model group (Figure 2E). In addition, Masson's and Sirius red staining revealed that, compared with those in the sham-operated group, the renal tissue of the rats in the model group presented with collagen fiber deposition. This fibrosis was significantly reduced by XHF treatment compared to the model group (Figure 2E). These findings demonstrate that XHF reduced renal inflammation, ameliorated interstitial fibrosis, and improved renal function in CKD rats.

To further evaluate the ameliorative effect of XHF on renal fibrosis, we assessed fibrosis marker proteins, including FN, vimentin and α-SMA, by Western blotting. Their abnormal increase indicated enhanced formation of the extracellular matrix (ECM), promoting fibrosis. Western blot analysis revealed significant increases in the expression of these fibrotic markers in the renal tissues of the 5/6 (A/I) model group compared to the sham group. These elevated protein levels were significantly reduced by XHF treatment (Figure 2F–I). To further evaluate the role of XHF in renal tubular function, we used Western blotting to detect organic anion transporter 3 (OAT3), Na^+/K^+-ATPase (ATP1B1), and aquaporin 1 (AQP1). These proteins play key roles in renal tubular epithelial cells: AQP1 is responsible for water reabsorption, OAT3 is involved in the transport of organic anions, and ATP1B1 is an essential component of the Na^+/K^+-ATPase pump, which establishes the electrochemical gradient driving many tubular functions.[23] Western blot analysis revealed no significant difference in OAT3 expression between the sham and 5/6 (A/I) model groups (Figure 2J and K). In contrast, ATP1B1 and AQP1 expression was significantly downregulated in the model compared to the sham group

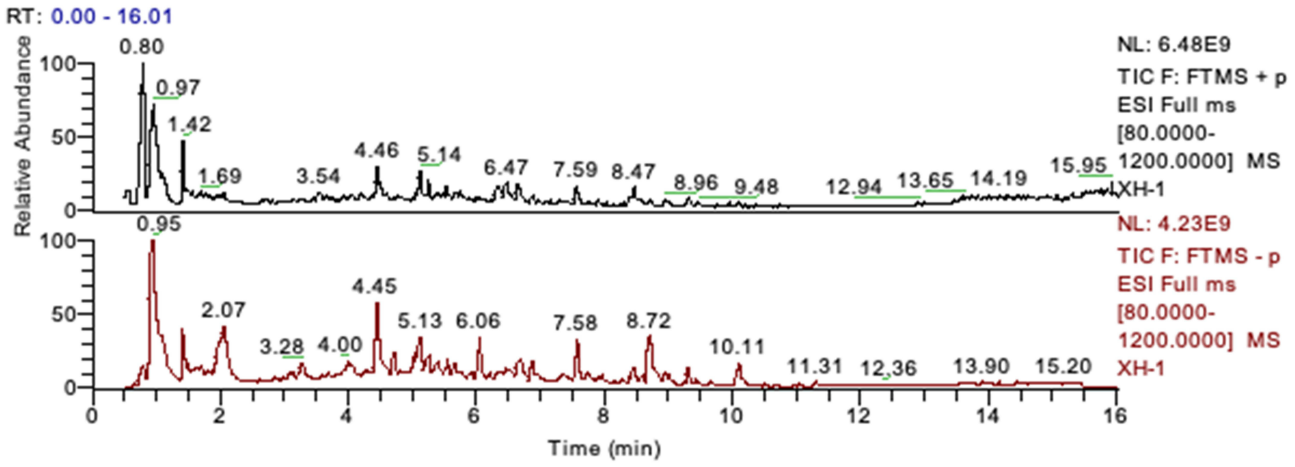

Figure 1 Mass analysis of XHF by UHPLC-Q-Orbitrap HRMS. Fingerprints of standard extracts of XHF mixtures by UHPLC-Q-Orbitrap HRMS in positive and negative ion mode.

https://doi.org/10.2147/DDDT.S522318

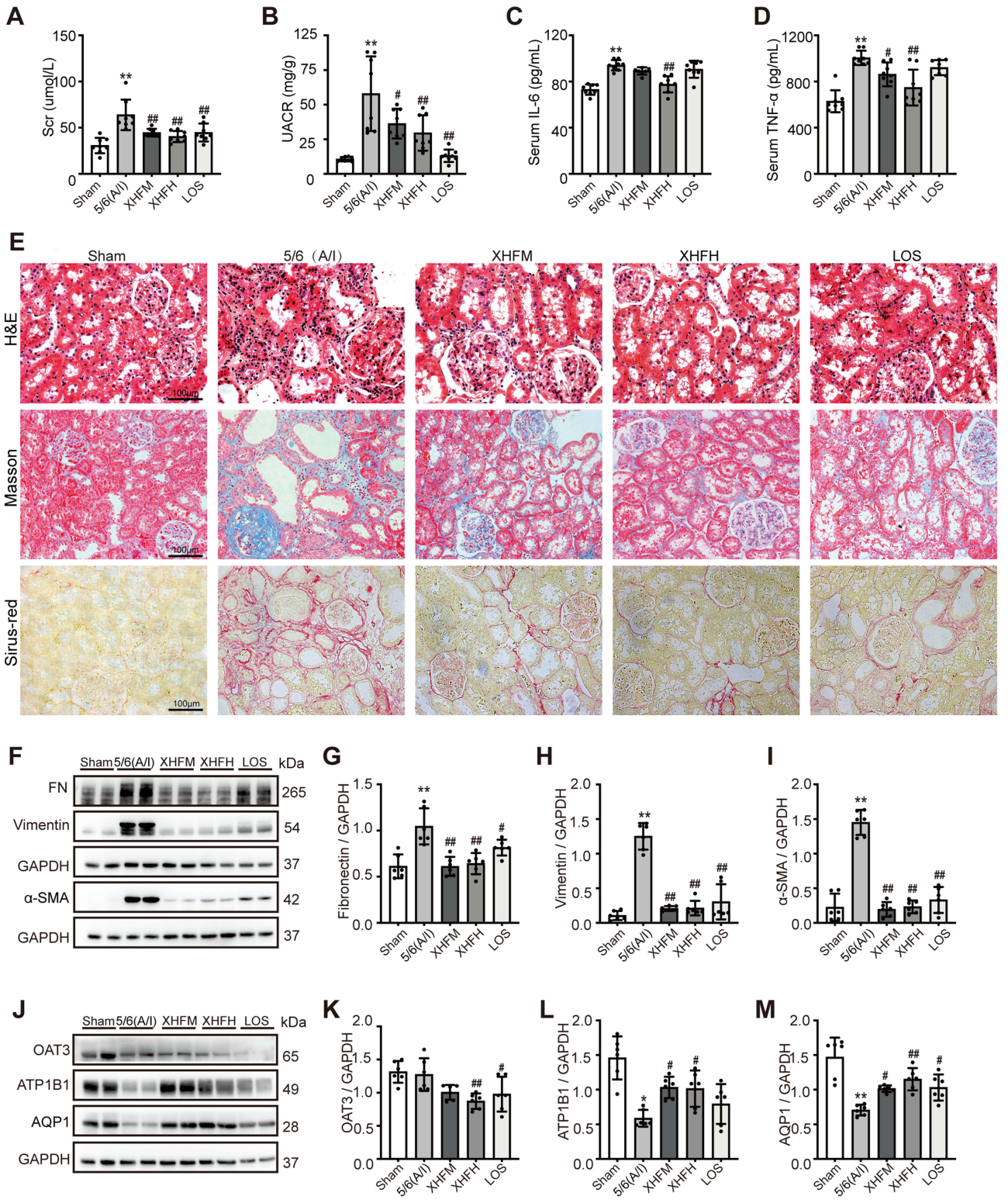

Figure 2 XHF ameliorates renal fibrosis and modulates water channel protein expression in 5/6 (A/I) nephrectomy-induced CKD rats. (**A**) Serum creatinine (Scr) levels. (**B**) Urinary albumin-to-creatinine ratio (UACR). (**C** and **D**) Serum inflammatory cytokine levels: (**C**) IL-6 and (**D**) TNF-α. (**E**) Representative images of renal histopathology (HE, Masson and Sirius red staining; Magnification × 200, Bar = 100 μm). (**F**) Western blot analysis of fibrotic markers (FN, vimentin, α-SMA) in kidney tissues. (**G–I**) Quantification of fibrotic protein expression (n=6) corresponding to (**F**). (**J**) Western blot analysis of solute transporters (OAT3, ATP1B1) and water channel protein (AQP1). (**K–M**) Quantification of transporter/channel protein expression corresponding to (**J**). Data are presented as mean ± SD (n=6). $^{*}p < 0.05$, $^{**}p < 0.01$, vs Sham group; $^{\#}p < 0.05$, $^{\#\#}p < 0.01$, vs 5/6 (A/I) group. Sham: sham-operated group; 5/6 (A/I): model group.

 https://doi.org/10.2147/DDDT.S522318

(Figure 2J, 2 and M). Importantly, XHF treatment significantly restored the expression of both ATP1B1 and AQP1 compared to the model group (Figure 2L and M).

Common Targets of XHF and CKD Analysis

We used PubChem for target prediction, and after removing duplicates, a total of 139 targets were obtained, which were merged and deduplicated via the Gene Cards, OMIM, DisGeNET, and other databases. Then, the overlapping targets of CKD and XHF were intersected using VennyGeneCards, and a total of 119 targets were obtained (Figure 3A). A PPI network (178 nodes, 504 edges) constructed from these targets revealed PKCδ as a top hub protein based on node centrality, alongside CYP1B1, SRC, AKT1, PIK3CB, and ESR1 (Figure 3B). In addition, the core target information was entered into the DAVID database for KEGG pathway and GO analyses (Figure 3C and D). Collectively, network pharmacology predicts XHF-mediated amelioration of renal fibrosis and CKD progression primarily through PKCδ signaling pathway inhibition, with concomitant suppression of fibrosis-associated pathways.

XHF Ameliorates Renal Fibrosis by Inhibiting PKCδ and MAPK Signaling Pathways

In this study, we further investigated whether XHF could alleviate HK-2 cell injury and its TGF-β1-induced fibrotic phenotype. Based on CCK-8 cell viability assays, we identified TGF-β1 concentrations (5 ng/mL and 10 ng/mL) with minimal impact on cellular metabolic activity (Figure 4A) and safe concentrations of XHF (5, 10, or 20 μM) (Figure 4B). Subsequent Western blotting and IF staining analyses revealed that 5 ng/mL TGF-β1 significantly inhibited HK-2 cell proliferation (reduced Ki-67) and induced a fibrotic phenotype (elevated vimentin expression), successfully establishing a dual phenotype characterized by proliferation suppression and fibrosis. Both XHF and the PKCδ inhibitor rottlerin (1 μM) effectively ameliorated this phenotype (Figure 4C–H). Although network pharmacology analysis suggested a potential role for the AGE-RAGE signaling pathway, our experimental validation in this model, based on protein-

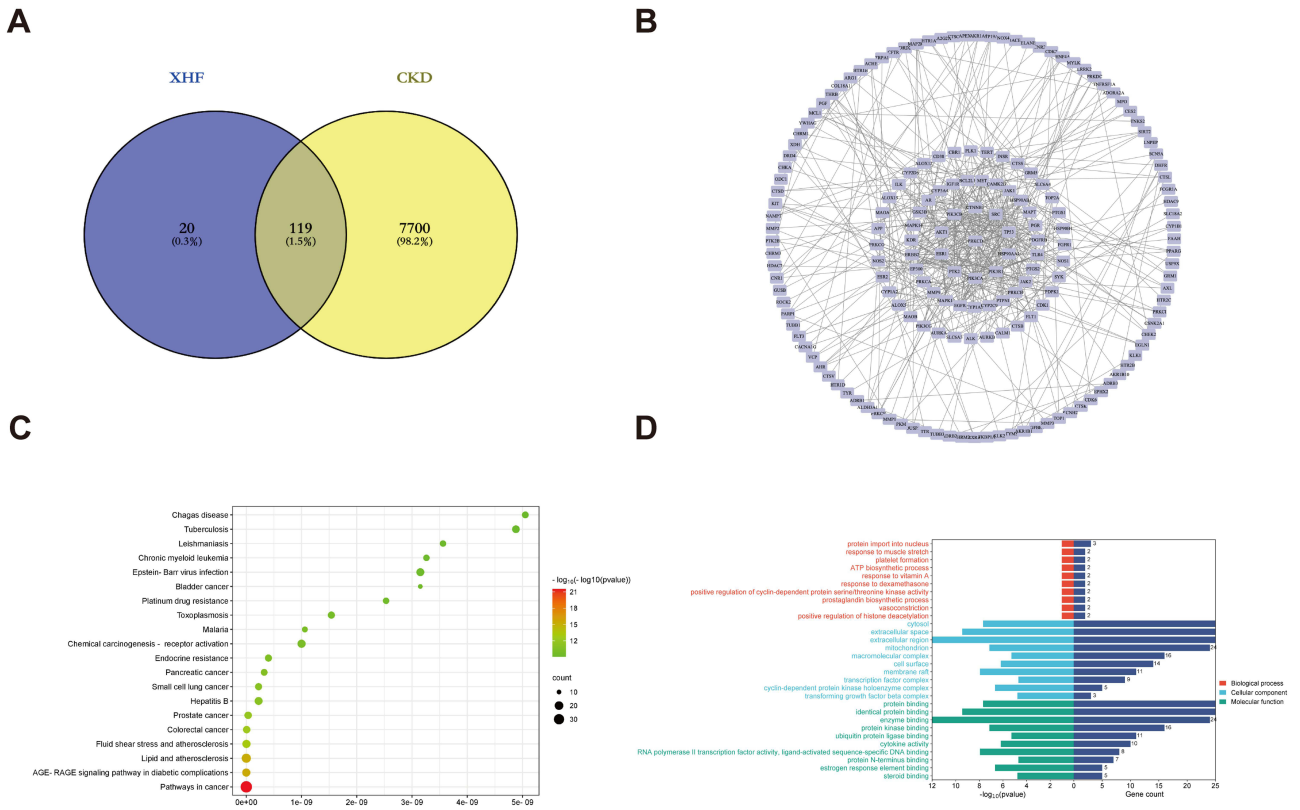

Figure 3 Common targets and functional enrichment analysis for XHF in CKD. (**A**) A total of 119 overlapping protein targets were identified between XHF and CKD. (**B**) PPI network. (**C**) Enrichment results for the top 20 KEGG pathways. (**D**) GO term enrichment. Top biological processes (BP, upper); Top cellular components (CC, middle); Top molecular functions (MF, lower).

https://doi.org/10.2147/DDDT.S522318

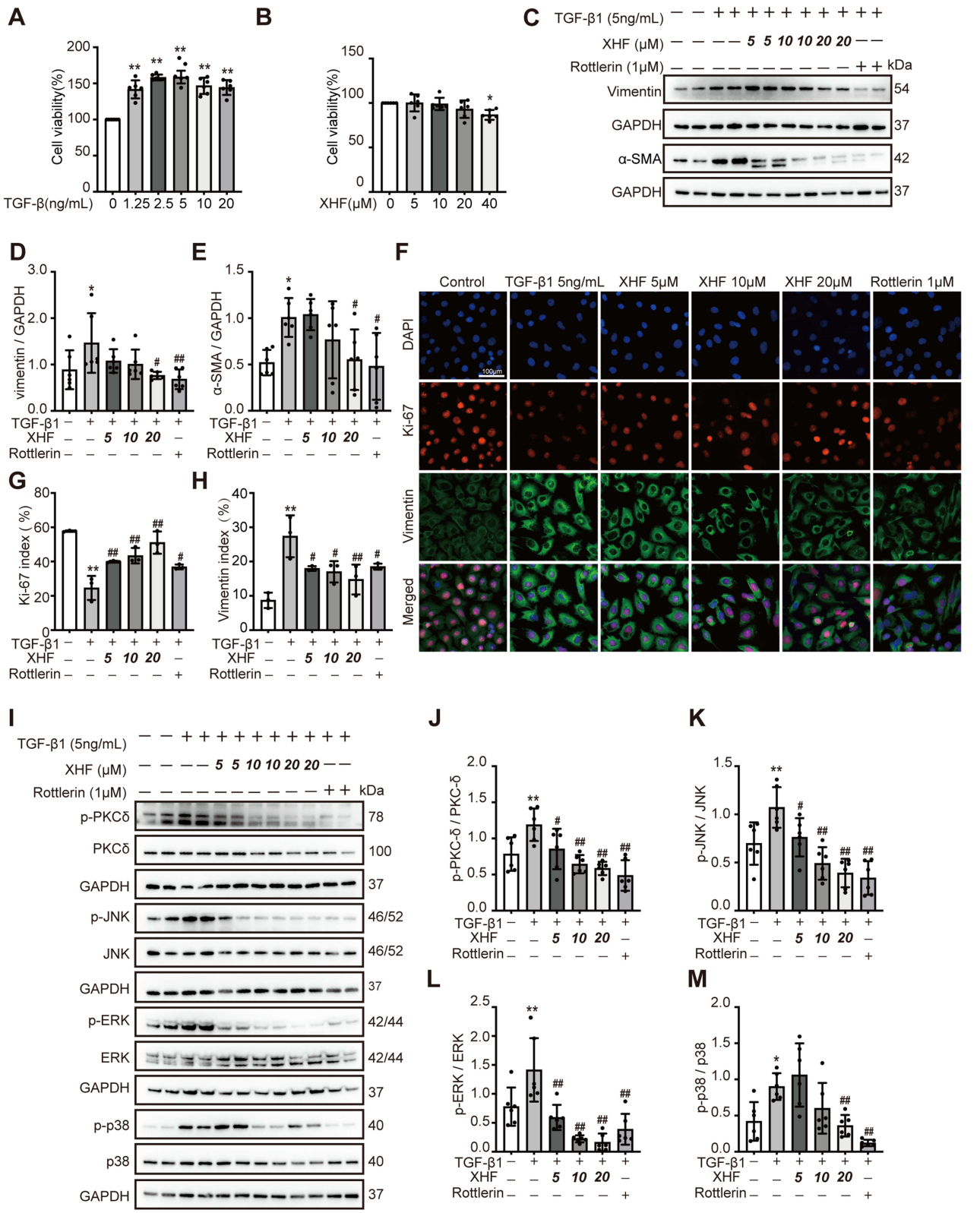

Figure 4 XHF ameliorates TGF-β1-induced fibrosis and modulates PKCδ and its signaling pathways in HK-2 cells. (**A**) Viability of HK-2 cells treated with varying concentrations of TGF-β1 for 48 hours. (**B**) Viability of HK-2 cells treated with varying concentrations of XHF for 48 hours. (**C**) HK-2 cells were cultured with 5 ng/mL TGF-β1 and treated with 5, 10, or 20 μM XHF and 1 μM Rottlerin for 48 hours. Proteins were collected, and Western blot analysis was used to detect the expression of vimentin and α-SMA in each group. (**D** and **E**) Quantification of vimentin and α-SMA protein expression levels from (**C**) (n=6). (**F**–**H**) Immunofluorescence staining of Ki-67 (cell proliferation) and vimentin (fibrosis severity) in HK-2 cells, with DAPI nuclear counterstain (Magnification × 200, Bar = 100 μm; n=3). (**I**) Western blot analysis of p-PKCδ, PKCδ, p-JNK, and JNK, p-ERK, ERK, p-p38 and p38 expression in HK-2 cells from each group. (**J**–**M**) Quantification of p-PKCδ, p-JNK, p-ERK, and p-p38 protein expression levels from (**I**). Data are presented as mean ± SD. *$p < 0.05$, **$p < 0.01$, vs control group; $^{\#}p < 0.05$, $^{\#\#}p < 0.01$, vs TGF-β1 group.

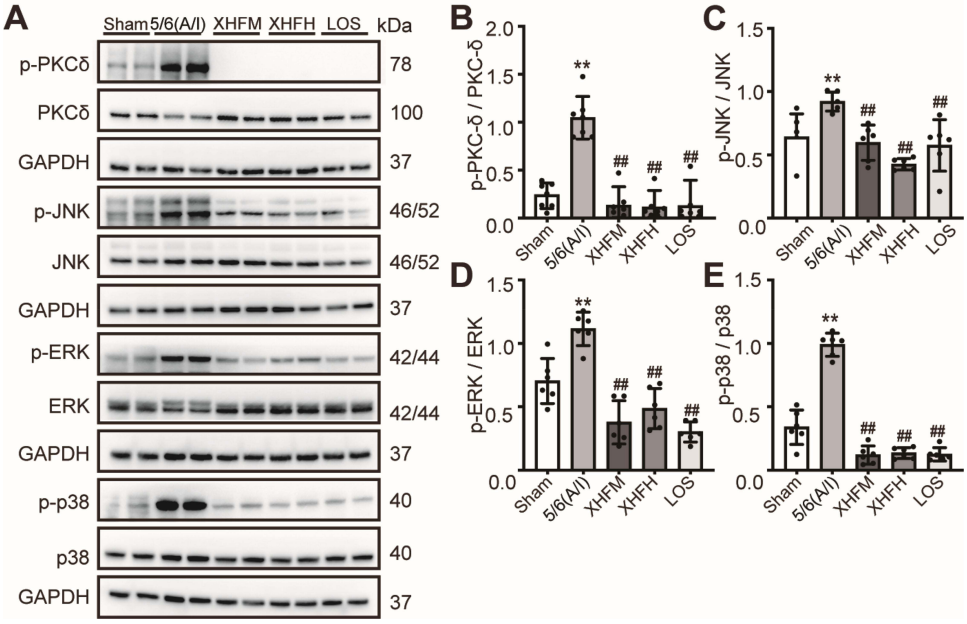

Figure 5 XHF attenuates PKCδ activation and downstream signaling pathways in the kidney tissue of 5/6 (A/I) nephrectomy-induced CKD rats. (**A**) SD rats were acclimatized and treated for 1 week with 5/6 nephrectomy, and after 4 weeks, the model rats were randomly divided into four groups: 5/6 (A/I), XHFM, XHFH, and LOS. After 8 weeks of treatment, kidney tissues were collected at the end of the experiment. Representative Western blot images showing protein expression levels of p-PKCδ, PKCδ, p-JNK, JNK, p-ERK, ERK, p-p38, and p38 in kidney tissues. (**B**–**E**) Quantitative analysis of the relative protein expression levels (phosphorylated/total ratio) of (**B**) p-PKCδ/PKCδ, (**C**) p-JNK/JNK, (**D**) p-ERK/ERK, and (**E**) p-p38/p38 corresponding to (**A**). Data are presented as mean ± SD (n=6). $^{**}p < 0.01$, vs Sham group; $^{\#\#}p < 0.01$, vs 5/6 (A/I) group. Sham: sham-operated group; 5/6 (A/I): model group.

protein interaction (PPI) network analysis, identified the PKCδ and its downstream MAPK pathway as the more significant targets regulated by XHF. Results demonstrated that both XHF and rottlerin suppressed TGF-β1-induced activation of the PKCδ Tyr311 phosphorylation site and significantly inhibited the phosphorylation levels of JNK, ERK, and p38 MAPK (Figure 4I–M). Notably, consistent results were observed in kidney tissues from 5/6 (A/I) nephrectomy model rats (Figure 5A–E), further validating this mechanism in vivo. Collectively, our data indicate that XHF alleviates renal fibrosis primarily through suppressing PKCδ phosphorylation and subsequent MAPK pathway inhibition.

XHF Ameliorates Renal Fibrosis by Inhibiting Endoplasmic Reticulum (ER) Stress and Cellular Senescence in 5/6 (A/I) Rats

Since ER stress is a key factor in promoting cellular senescence, we evaluated the effects of XHF on both ER stress and cellular senescence simultaneously. We investigated the effects of XHF on the expression of the ER stress-related proteins BIP and CHOP, the protein expression levels of p53/p21 pathway proteins, and the expression of SASP-related factors in rat kidney tissue in the 5/6 (A/I) model. First, Western blot results revealed that, compared to the sham group, the expression of the ER-stress chaperone BIP was significantly decreased, while the pro-apoptotic marker CHOP was markedly elevated in the renal tissue of model rats. Treatment with different doses of XHF did not significantly alter the reduced BIP levels observed in the model group, but XHFM and XHFH significantly attenuated the CHOP up-regulation (Figure 6A–C). Western blot analysis also revealed activation of the p53/p21 cell cycle arrest pathway in the renal tissues of 5/6 (A/I) model rats; notably, XHFM and XHFH all significantly inhibited this activation (Figure 6A, D and E). We next assessed the expression of NF-κB and the SASP-secreted factor IL-6, and our results revealed that the levels of p-NF-κB and IL-6 were significantly greater in the 5/6 (A/I) model rats than in the sham rats. Importantly, specific doses of XHF treatment (as indicated by statistical significance markers in Figure 6G and H) significantly reduced p-NF-κB and IL-6 levels (Figure 6F and H). In addition, SA-β-gal staining revealed a significant increase in the proportion of SA-β-gal positive cells in the renal tissues of the 5/6 A/I model rats compared with the sham group. Notably, XHFH treatment significantly reduced the proportion of SA-β-gal positive cells in renal tissue (Figure 6I and J). These findings indicate

https://doi.org/10.2147/DDDT.S522318

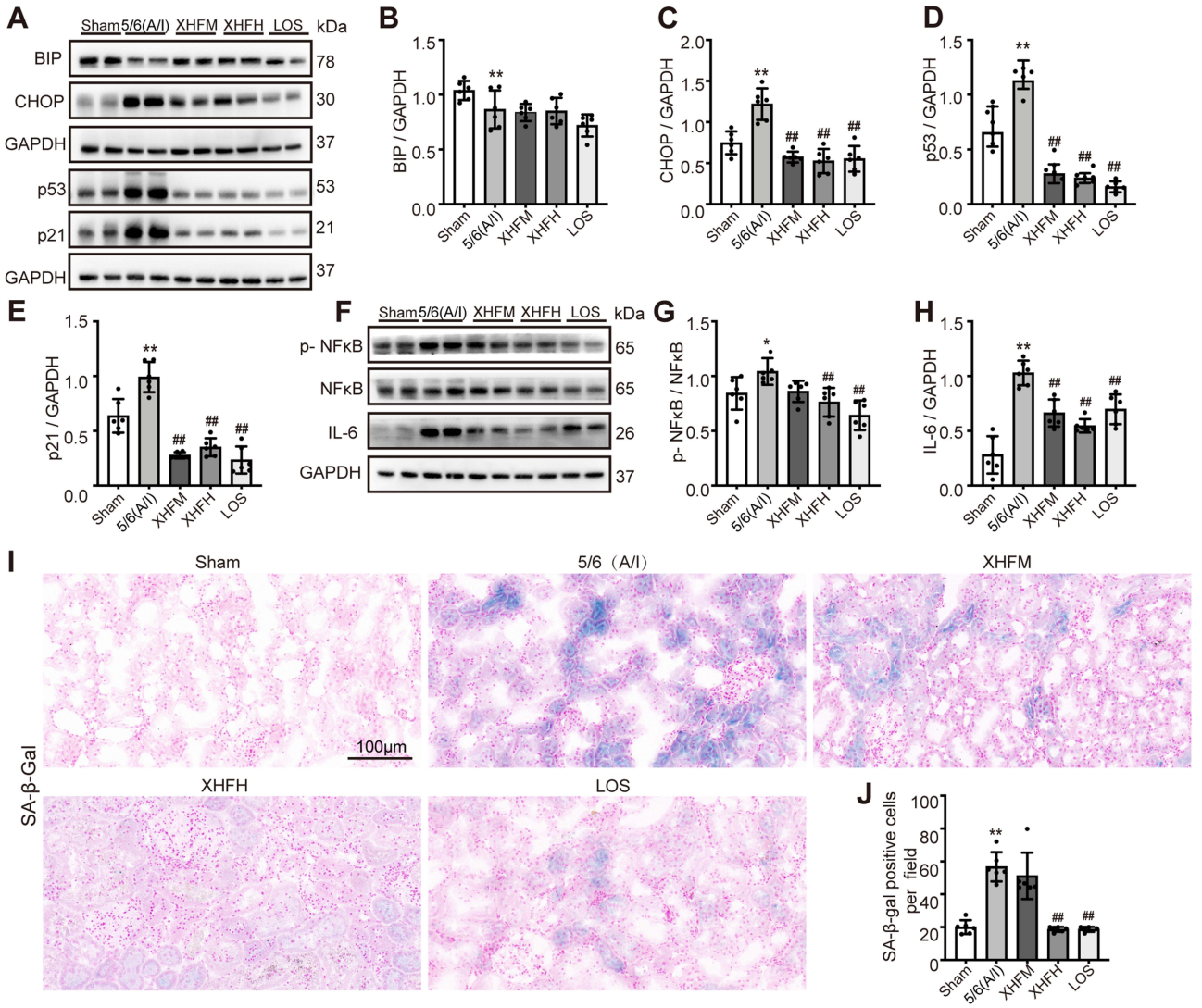

Figure 6 XHF mitigates ER stress, cellular senescence and SASP-associated inflammation in renal tissue of CKD rats induced by 5/6 (A/I) nephrectomy. (**A**) Western blot analysis of endoplasmic reticulum stress markers (BIP, CHOP) and senescence-associated proteins (p53, p21). (**B**–**E**) Quantification of (**B**) BIP, (**C**) CHOP, (**D**) p53, and (**E**) p21 protein levels from (**A**). (**F**) Western blotting was used to detect the protein expression of p-NF-κB, NF-κB, and IL-6. (**G**) p-NF-κB/NF-κB ratio and (**H**) IL-6 levels corresponding to (**F**). (**I**) SA-β-gal staining in renal sections (Magnification × 200, Bar = 100 μm). (**J**) Quantitative analysis of SA-β-gal positive cells in (**I**). Data are presented as mean ± SD (n=6). $^{*}p < 0.05$, $^{**}p < 0.01$, vs Sham group; $^{\#\#}p < 0.01$, vs 5/6 (A/I) group. Sham: sham-operated group; 5/6 (A/I): model group.

that XHF ameliorates cellular senescence and associated SASP/inflammation. These findings indicate that XHF ameliorates cellular senescence.

XHF Inhibits ER Stress and Senescence in TGF-β1-Induced HK-2 Cells

Building upon our in vivo findings in the 5/6 (A/I) model (Figure 6), where XHF ameliorated renal fibrosis through attenuating cellular senescence, we employed an in vitro TGF-β1-stimulated HK-2 cell model to mechanistically probe the role of cellular senescence in XHF's action. In this established fibrotic model, TGF-β1 stimulation robustly induced key pathological features: significant upregulation of ER stress markers BIP and CHOP (Figure 7A–C), increased expression of the senescence marker p21 (Figure 7A and D), activation of the SASP-regulating transcription factor NF-κB, enhanced secretion of the canonical SASP factor IL-6 (Figure 7E–G), and a marked increase in SA-β-gal-positive senescent cells (Figure 7H and I). Both XHF and Rottlerin significantly attenuated these TGF-β1-induced alterations, suppressing BIP and CHOP expression (Figure 7B and C), reducing p21 levels (Figure 7D), inhibiting p-NF-κB and IL-6 secretion (Figure 7F and G), and decreasing SA-β-gal-positive cells (Figure 7H and I). Notably, co-treatment

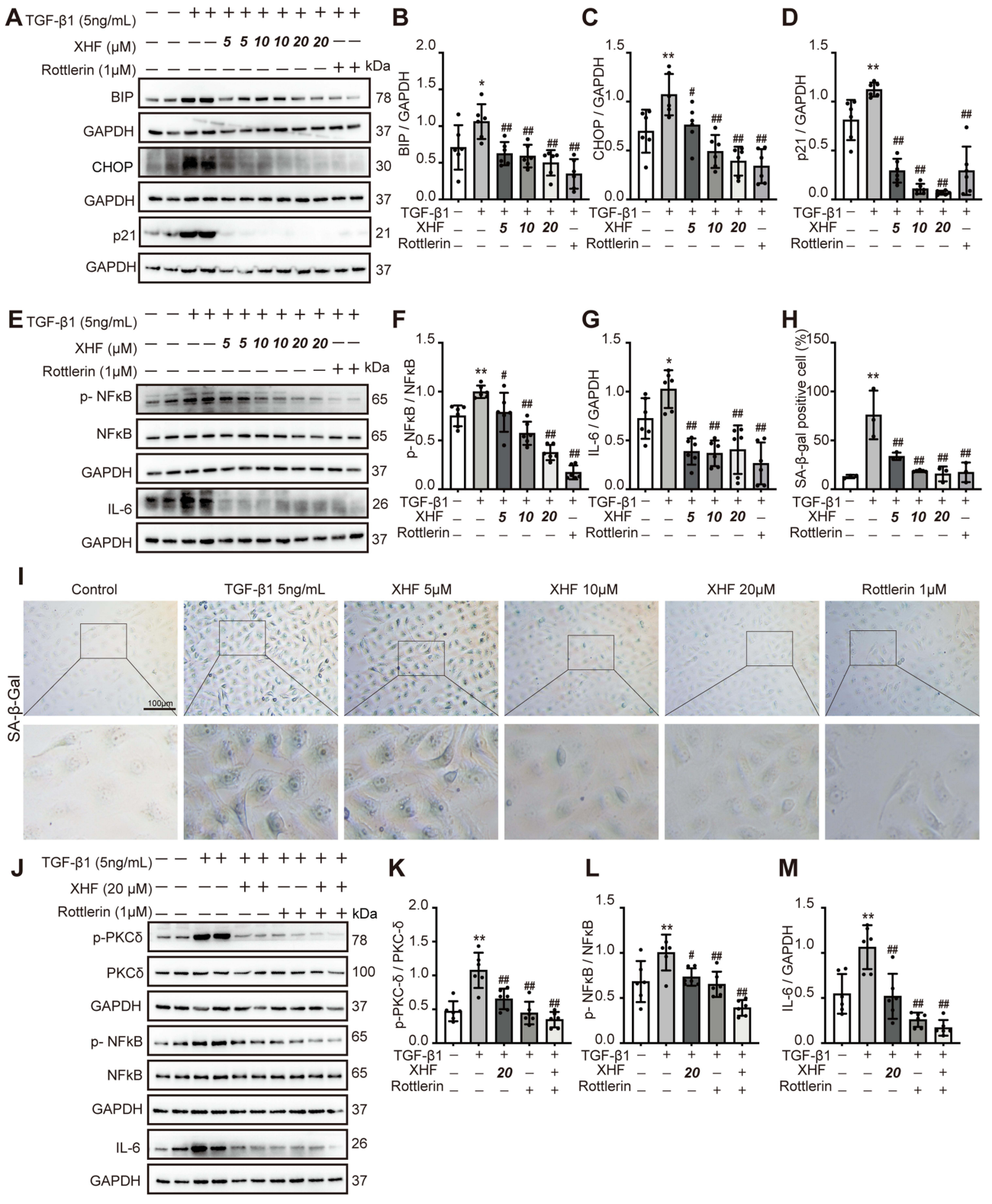

Figure 7 XHF attenuates TGF-β1-induced ER stress and cellular senescence in HK-2 cells. (**A**) Western blot analysis of ER stress markers (BIP, CHOP) and senescence marker p21 in HK-2 cells that were cultured with 5 ng/mL TGF-β1 and treated with 5, 10, or 20 μM XHF and 1 μM Rottlerin for 48 hours. (**B**–**D**) Quantification of (**B**) BIP, (**C**) CHOP, and (**D**) p21 protein levels corresponding to (**A**) (n=6). (**E**) Western blot detection of p-NF-κB, NF-κB, and IL-6 in HK-2 cells. (**F** and **G**) Quantification of (**F**) p-NF-κB/NF-κB ratio and (**G**) IL-6 levels corresponding to (**E**) (n=6). (**H**) Quantification of SA-β-gal-positive cells based on staining in (**I**) (n=3). (**I**) SA-β-gal staining in HK-2 cells. (Magnification × 200, Bar = 100 μm). The lower panels are magnifications of the black-colored squared box shown in the upper panels. (**J**) Western blot analysis of PKCδ/NF-κB signaling in HK-2 cells treated with: TGF-β1 (5 ng/mL), XHF (20 μM), Rottlerin (1 μM), or XHF (20 μM) + Rottlerin (1 μM) for 48 h. (**K**–**M**) Quantification of (**K**) p-PKCδ/PKCδ ratio, (**L**) p-NF-κB/NF-κB ratio, and (**M**) IL-6 levels corresponding to (**J**) (n=6). Data are presented as mean ± SD. $^{*}p < 0.05$, $^{**}p < 0.01$, vs control group; $^{\#}p < 0.05$, $^{\#\#}p < 0.01$, vs TGF-β1 group.

https://doi.org/10.2147/DDDT.S522318

with 20 μM XHF and Rottlerin produced greater inhibition of p-PKCδ, p-NF-κB, and IL-6 expression compared to individual treatments (Figure 7J–M).

Discussion

This study aims to explore the anti-fibrotic mechanisms of XHF, with a particular focus on its potential regulatory effects on cellular senescence in the context of RIF. By combining network pharmacology predictions and experimental validation, we identified PKCδ as a key potential target of XHF. Our results showed that XHF administration significantly ameliorated renal interstitial fibrosis, inflammation, and tubular injury in the 5/6 nephrectomy (A/I) rat model. Importantly, XHF treatment effectively inhibited the phosphorylation of PKCδ both in vivo and in vitro. This inhibition was associated with the suppression of the downstream MAPK signaling pathway (JNK, ERK, p38) and a reduction in key SASP factors, especially IL-6. Collectively, our findings suggest that PKCδ is a core target of XHF's anti-RIF protective effects, with the potential mechanism being the alleviation of PKCδ-driven cellular senescence phenotypes.

Renal fibrosis is a common pathway in multiple kidney diseases, and antifibrosis remains a major focus and challenge in the treatment of CKD.[24] Accumulating evidence indicates that cellular senescence occurs not only in naturally aging kidneys but also participates in driving the progression of fibrosis in renal injury.[25,26] Senescent cells exhibit irreversible cell cycle arrest, mediated predominantly by p21 activation (typically via the p53/p21 axis) in response to diverse CKD-associated stressors, including oxidative stress, metabolic dysregulation, and notably, ER stress. Additional hallmarks include expression of SA-β-Gal and secretion of pro-fibrotic SASP factors, such as IL-6 and TGF-β1. These factors promote chronic inflammation and excessive deposition of ECM components, such as α-SMA and fibronectin, which ultimately exacerbate the processes of renal inflammation and excessive fibrosis.[27,28] We observed significant signs of senescence, including activation of the p21 pathway, increased SA-β-Gal activity, and elevated IL-6 levels, in both the TGF-β1-induced HK-2 cell model and the 5/6 nephrectomy (A/I) rat model of renal interstitial fibrosis. These findings are consistent with those of other researchers.[29,30] XHF administration effectively alleviated these senescence-associated markers.

PKCδ has become a molecule of significant interest in renal pathology. Studies show that PKCδ expression is upregulated in the renal tubules of CKD patients and in rodent fibrosis models. Its knockdown is associated with improved mitochondrial function, enhanced repair of renal tubular cells, and reduced SASP.[31,32] While initial network pharmacology analysis suggested possible involvement of the AGE-RAGE pathway, our experimental validation prioritized PKCδ due to its established relevance in senescence and fibrosis. We demonstrated that XHF significantly inhibited the phosphorylation of PKCδ (Tyr311) in the fibrotic milieu. This inhibition was associated with reduced phosphorylation of key MAPK family members (JNK, ERK, p38) and the NF-κB p65 subunit, NF-κB activation is a well-established driver of pro-inflammatory cytokine production.[33] IL-6 is a potent mediator that acts in an autocrine/paracrine manner to promote fibrosis.[34,35] These correlative findings support the hypothesis that PKCδ acts as an upstream regulator, orchestrating a signaling network involving MAPK, NF-κB, and ultimately IL-6 secretion, which is associated with fibrosis-associated senescence. The rottlerin experiments provide pharmacological evidence supporting PKCδ's role in activating NF-κB in our cellular model. Nevertheless, while rottlerin experiments provide pharmacological evidence supporting PKCδ's role, its off-target effects necessitate complementary genetic approaches in future studies.

In summary, this study provides evidence that XHF attenuates RIF in established experimental models. We identified PKCδ as a key potential target of XHF and demonstrated that XHF inhibits PKCδ phosphorylation. Our findings further suggest an association between PKCδ inhibition and the suppression of downstream MAPK/NF-κB signaling, leading to reduced levels of the critical SASP factor IL-6 and attenuation of cellular senescence markers (p21, SA-β-Gal) observed within the fibrotic milieu. These results establish PKCδ as a significant mediator potentially linking XHF treatment to the amelioration of fibrosis-associated cellular senescence and RIF progression. XHF warrants further investigation as a promising therapeutic candidate for CKD, with PKCδ representing a compelling mechanistic target for future validation.

Data Sharing Statement

Upon request to corresponding author, the data will be provided.

Ethics Approval

The human data in this study were sourced exclusively from public databases with open licenses permitting unrestricted reuse. Per China's National Science and Technology Ethics Committee guidelines, such data usage is exempt from ethical review (available at https://www.gov.cn/zhengce/zhengceku/2023-02/28/content_5743658.htm). Ethical exemption was confirmed by the Ethics Committee of Shuguang Hospital, affiliated with Shanghai University of Traditional Chinese Medicine.

Author Contributions

All authors made a significant contribution to the work reported, whether that is in the conception, study design, execution, acquisition of data, analysis and interpretation, or in all these areas; took part in drafting, revising or critically reviewing the article; gave final approval of the version to be published; have agreed on the journal to which the article has been submitted; and agree to be accountable for all aspects of the work.

Funding

This research was supported by the National Natural Science Foundation of China(82174289, 81973807), the Shanghai Magnolia Talent Plan Pujiang Project (24PJD112), the Science and Technology Development Project of Shanghai Academy of Traditional Chinese Medicine (24YJS05).

Disclosure

The authors report no conflicts of interest in this work.

References

1. Dorgelo A, Oostrom Ta J. An integrated approach towards a public health perspective on chronic kidney disease. *Nat Rev Nephrol*. 2022;18(3):131–132. doi:10.1038/s41581-022-00537-4
2. Bikbov B, Purcell CA, Levey AS. Global, regional, and national burden of chronic kidney disease, 1990-2017: a systematic analysis for the global burden of disease study 2017. *Lancet*. 2020;395(10225):709–733. doi:10.1016/s0140-6736(20)30045-3
3. Miguel V, Tituaña J, Herrero JI, et al. Renal tubule cpt1a overexpression protects from kidney fibrosis by restoring mitochondrial homeostasis. *J Clin Invest*. 2021;131(5). doi:10.1172/jci140695
4. Grgic I, Campanholle G, Bijol V, et al. Targeted proximal tubule injury triggers interstitial fibrosis and glomerulosclerosis. *Kidney Int*. 2012;82(2):172–183. doi:10.1038/ki.2012.20
5. Gewin L, Zent R, Pozzi A. Progression of chronic kidney disease: too much cellular talk causes damage. *Kidney Int*. 2017;91(3):552–560. doi:10.1016/j.kint.2016.08.025
6. Ding X, Ren Y, He X. Ifn-i mediates lupus nephritis from the beginning to renal fibrosis. *Front Immunol*. 2021;12:676082. doi:10.3389/fimmu.2021.676082
7. Liu BC, Tang TT, Lv LL, et al. Renal tubule injury: a driving force toward chronic kidney disease. *Kidney Int*. 2018;93(3):568–579. doi:10.1016/j.kint.2017.09.033
8. Meng XM, Nikolic-Paterson DJ, Lan HY. Inflammatory processes in renal fibrosis. *Nat Rev Nephrol*. 2014;10(9):493–503. doi:10.1038/nrneph.2014.114
9. Liu X, Zhan P, Zhang Y, et al. Lysosomal-associated protein transmembrane 5, tubular senescence, and progression of ckd. *J Am Soc Nephrol*. 2024;35(12):1655–1670. doi:10.1681/asn.0000000000000446
10. Wu Q, Chen Q, Xu D, et al. C-x-c chemokine receptor type 4 promotes tubular cell senescence and renal fibrosis through β-catenin-inhibited fatty acid oxidation. *J Cell Mol Med*. 2024;28(3):e18075. doi:10.1111/jcmm.18075
11. Chen Y, Yang L. Cellular senescence in renal ischemia-reperfusion injury. *Chin Med J*. 2025;138(15):1794–1806. doi:10.1097/cm9.0000000000003698
12. Baisantry A, Berkenkamp B, Rong S, et al. Time-dependent p53 inhibition determines senescence attenuation and long-term outcome after renal ischemia-reperfusion. *Am J Physiol Renal Physiol*. 2019;316(6):F1124–f32. doi:10.1152/ajprenal.00333.2018
13. Yang M, Wu S, Dai Q, et al. Andrographolide prevents renal fibrosis via decelerating lipotoxicity-mediated premature senescence of tubular epithelial cells. *Biochem Pharmacol*. 2024;230(Pt 3):116615. doi:10.1016/j.bcp.2024.116615
14. Rovillain E, Mansfield L, Caetano C, et al. Activation of nuclear factor-kappa b signalling promotes cellular senescence. *Oncogene*. 2011;30(20):2356–2366. doi:10.1038/onc.2010.611
15. Khan D, Zhou H, You J, et al. Tobacco smoke condensate-induced senescence in endothelial cells was ameliorated by colchicine treatment via suppression of nf-κb and mapks p38 and erk pathways activation. *Cell Commun Signal*. 2024;22(1):214. doi:10.1186/s12964-024-01594-x

16. Yang L, Wang M, Zhou Y, et al. Shen Shuai ii recipe attenuates renal interstitial fibrosis by improving hypoxia via the il-1β/c-myc pathway. *Evid Based Complement Alternat Med*. 2021;2021:5539584. doi:10.1155/2021/5539584
17. Feng HY, Wang YQ, Yang J, et al. Anthraquinones from rheum officinale ameliorate renal fibrosis in acute kidney injury and chronic kidney disease. *Drug Des Devel Ther*. 2025;19:5739–5760. doi:10.2147/dddt.S521265
18. Qian HQ, Wu DC, Li CY, et al. A systematic review of traditional uses, phytochemistry, pharmacology and toxicity of epimedium koreanum Nakai. *J Ethnopharmacol*. 2024;318(Pt B):116957. doi:10.1016/j.jep.2023.116957
19. Wang M, Wang L, Zhou Y, et al. Icariin attenuates renal fibrosis in chronic kidney disease by inhibiting interleukin-1β/transforming growth factor-β-mediated activation of renal fibroblasts. *Phytother Res*. 2021;35(11):6204–6215. doi:10.1002/ptr.7256
20. Xu L, Gao J, Huang D, et al. Emodin ameliorates tubulointerstitial fibrosis in obstructed kidneys by inhibiting ezh2. *Biochem Biophys Res Commun*. 2021;534:279–285. doi:10.1016/j.bbrc.2020.11.094
21. Lu YP, Wu HW, Zhu T, et al. Empagliflozin reduces kidney fibrosis and improves kidney function by alternative macrophage activation in rats with 5/6-nephrectomy. *Biomed Pharmacother*. 2022;156:113947. doi:10.1016/j.biopha.2022.113947
22. Li X, Pabla N, Wei Q, et al. Pkc-delta promotes renal tubular cell apoptosis associated with proteinuria. *J Am Soc Nephrol*. 2010;21(7):1115–1124. doi:10.1681/asn.2009070760
23. Verma SK, Molitoris BA. Renal endothelial injury and microvascular dysfunction in acute kidney injury. *Semin Nephrol*. 2015;35(1):96–107. doi:10.1016/j.semnephrol.2015.01.010
24. Li YQ, Yu XM, Shang XM, et al. Biochanin a suppresses klf6-mediated smad3 transcription to attenuate renal fibrosis in uuo mice. *Phytomedicine*. 2024;135:156067. doi:10.1016/j.phymed.2024.156067
25. Miao J, Liu J, Niu J, et al. Wnt/β-catenin/ras signaling mediates age-related renal fibrosis and is associated with mitochondrial dysfunction. *Aging Cell*. 2019;18(5):e13004. doi:10.1111/acel.13004
26. Braun H, Schmidt BM, Raiss M, et al. Cellular senescence limits regenerative capacity and allograft survival. *J Am Soc Nephrol*. 2012;23(9):1467–1473. doi:10.1681/asn.2011100967
27. Huang Q, Zhong K, Wei J. Circpwwp2a promotes renal interstitial fibrosis through modulating mir-182/rock1 axis. *Ren Fail*. 2024;46(2):2396455. doi:10.1080/0886022x.2024.2396455
28. Gao P, Zou X, Sun X, et al. Cellular senescence in metabolic-associated kidney disease: an update. *Cells*. 2022;11(21):3443. doi:10.3390/cells11213443
29. Xiao PT, Hao JH, Kuang YJ, et al. Targeting neuraminidase 4 attenuates kidney fibrosis in mice. *Adv Sci*. 2024;11(39):e2406936. doi:10.1002/advs.202406936
30. Liu C, Wang X, Wang X, et al. A new lkb1 activator, piericidin analogue s14, retards renal fibrosis through promoting autophagy and mitochondrial homeostasis in renal tubular epithelial cells. *Theranostics*. 2022;12(16):7158–7179. doi:10.7150/thno.78376
31. Wang D, Li Y, Li G, et al. Inhibition of pkc-δ retards kidney fibrosis via inhibiting cgas-sting signaling pathway in mice. *Cell Death Discov*. 2024;10(1):314. doi:10.1038/s41420-024-02087-z
32. Zhu J, Zhang G, Song Z, et al. Protein kinase c-δ mediates kidney tubular injury in cold storage-associated kidney transplantation. *J Am Soc Nephrol*. 2020;31(5):1050–1065. doi:10.1681/asn.2019101060
33. Liu YC, Chen SY, Chen YY, et al. Polysaccharides extracted from common buckwheat (Fagopyrum esculentum) attenuate cognitive impairment via suppressing rage/p38/nf-κb signaling and dysbiosis in alcl(3)-treated rats. *Int J Biol Macromol*. 2024;276(Pt 2):133898. doi:10.1016/j.ijbiomac.2024.133898
34. Kandhaya-Pillai R, Yang X, Tchkonia T, et al. TNF -α/ IFN -γ synergy amplifies senescence-associated inflammation and SARS-CoV-2 receptor expression via hyper-activated JAK/STAT1. *Aging Cell*. 2022;21(6):e13646. doi:10.1111/acel.13646
35. Xu D, Moru P, Liao K, et al. High glucose-induced senescence contributes to tubular epithelial cell damage in diabetic nephropathy. *Exp Gerontol*. 2024;197:112609. doi:10.1016/j.exger.2024.112609